Published in IET Communications
Received on 15th January 2012
Revised on 7th June 2012
doi: 10.1049/iet-com.2012.0029

ISSN 1751-8628

Design of isotropic orthogonal transform algorithm-based multicarrier systems with blind channel estimation

J. Du[1] *P. Xiao*[2] *J. Wu*[3] *Q. Chen*[4]

[1]*School of Electrical Engineering, Royal Institute of Technology (KTH), SE-100 44 Stockholm, Sweden*
[2]*Centre for Communication Systems Research (CCSR), Faculty of Engineering and Physical Sciences, University of Surrey Guildford, GU2 7XH, UK*
[3]*Bell Laboratories, Alcatel-Lucent Pudong Jinqiao, Shanghai 201206, People's Republic of China*
[4]*Key Lab of Information Coding and Transmission Southwest Jiaotong University, Chengdu 610031, People's Republic of China*
E-mail: p.xiao@surrey.ac.uk

Abstract: Orthogonal frequency division multiplexing (OFDM) technique has gained increasing popularity in both wired and wireless communication systems. However, in the conventional OFDM systems the insertion of a cyclic prefix (CP) and the transmission of periodic training sequences for purpose of channel estimation decrease the system's spectral efficiency. As an alternative to OFDM, isotropic orthogonal transform algorithm (IOTA)-based multicarrier system adopts a proper pulse shaping with good time and frequency localisation properties to avoid interference and maintain orthogonality in real field among sub-carriers without the use of CP. In this study, the authors propose linearly precoded IOTA-based multicarrier systems to achieve blind channel estimation by utilising the structure of auto-correlation and cross-correlation matrices introduced by precoding. The results show that the proposed IOTA-based multicarrier systems achieve better power and spectral efficiency compared with the conventional OFDM systems.

1 Introduction

Orthogonal frequency division multiplexing (OFDM) [1, 2] is well suited for broadband applications because of its robustness against multipath fading by transforming a frequency selective channel into parallel flat fading channels. The OFDM technique has been adopted in the majority of current and future communications standards, for example, asymmetric digital subscriber line (ADSL), digital audio/video broadcasting, power line communications (PLC), IEEE 802.11 WLAN system, IEEE 802.16 WiMAX, IEEE 802.22 WRAN and 3GPP LTE etc.

In conventional OFDM systems, quadrature phase shift keying (QPSK)/quadrature amplitude modulation (QAM) symbols are shaped with a rectangular window. In such a case, no pulse filtering is needed, and inter-symbol interference (ISI) and inter-carrier interference (ICI) are avoided by adding a cyclic prefix (CP) before data transmission. However, CP is not for free, it increases power consumption and reduces spectral efficiency. For example, in IEEE 802.11 and long term evolution (LTE) standards, only 80% of a sub-frame is used for data transmission.

One way to solve this problem is to adopt a proper pulse shaping (prototype) function, which is well localised in time and frequency so that the ISI and ICI can be combated efficiently without CP. In the meantime, this prototype function must also guarantee orthogonality between sub-carriers. Unfortunately, according to the Balian–Low theorem [3], orthogonal basis and compactly supported pulses cannot be achieved simultaneously for OFDM/QAM systems without CP. Functions satisfying these two conditions do exist, but the optimally localised ones only guarantee orthogonality on real values. This dilemma excludes pulse-shaping OFDM/QAM from the candidate list and brings an alternative scheme OFDM/OQAM [4, 5] into the scene.

With offset modulations, for example, OQPSK, OQAM, the orthogonality can be maintained with proper pulse shaping design. We need to choose pulses with good time and frequency localisation (TFL) properties. The localisation in time aims to limit ISI and the localisation in frequency aims to limit ICI caused for instance by Doppler effects. Among different prototype filters, such as half-cosine, root-raised-cosine [6], isotropic orthogonal transform algorithm (IOTA) [4, 5], extended Gaussian function (EGF) [7] etc. the localisation property is optimal with the IOTA function, which has the same shape in time and frequency domains. We refer to such kind of IOTA-based multicarrier system as IOTA system in the sequel.

In a point-to-point single-user scenario, IOTA has a higher complexity than OFDM, but the difference is not significant

since its complexity can be largely reduced by filter bank implementation [7–9]. Since CP is not required, the IOTA system leads to higher power and spectral efficiency compared with conventional OFDM systems. IOTA also has advantages over OFDM in time and frequency dispersive channels since it is more robust to frequency offset, Doppler effects etc. The TFL properties of IOTA makes it favourable for mobile applications. Furthermore, the assumption of a flat fading channel over each sub-carrier remains valid as long as the number of sub-carriers is chosen to be sufficiently large, and the equalisation of IOTA signals is similar to that of OFDM [10, 11].

In a multiuser system, the high sensitivity of OFDM to carrier frequency offset among different users and the need for interference cancellation (IC) methods to reduce this sensitivity lead to very complex and yet not very effective systems. In filter bank multicarrier (FBMC) systems such as IOTA, on the other hand, near-optimal performance is achieved without any additional signal processing, such asIC, because of the excellent frequency-localised filters employed in FBMC-based systems [12]. The added complexity arising from IC blocks in an OFDM-based system makes it significantly more complex than its IOTA counterpart.

IOTA and OFDM systems in a realistic mobile communication context (both time and frequency dispersive) have been compared in [13–15] where it was shown that the performance advantage of IOTA over OFDM can be up to 4.5 dB depending on different type of wireless propagation channels. This concurs with our experimental results illustrated in the following sections of this paper.

The performance of a communication system depends largely on its ability to retrieve an accurate measurement of the underlying channel. The estimated channel information is used to enable coherent data detection in order to combat the detrimental effect of fading. To this end, training sequences including pilots and preambles are widely employed in practical OFDM and IOTA systems to estimate or identify channel information. For example, preamble based channel estimation methods have been proposed in [16, 17] where the intrinsic interference has been utilised to assist the channel estimation, which can achieve up to 2.4 dB gain over OFDM in double dispersive channels.

However, periodic transmission of training sequences decreases spectral efficiency. Blind channel estimation schemes avoid the use of training sequences, which makes them good candidates for achieving high spectral efficiency and allows more data to be used for information transfer. In this paper, we will study blind channel estimation schemes for linearly precoded IOTA systems. Blind channel estimation is achieved at the receiver by using the structure of auto-correlation and cross-correlation matrices introduced by precoding [18]. To the best of our knowledge, linear precoding-based blind channel estimation has not yet been investigated for FBMC systems in general and IOTA systems in particular.

The remainder of this paper is organised as follows: in Section 2, a polyphase filter implementation of the MIMO-IOTA system is presented. In Section 3, we propose a linearly precoded multiple-input, multiple-output (MIMO)-IOTA system, which enables blind channel estimation in order to avoid the transmission of training sequence in addition to the elimination of CP. This is the main contribution of this paper. Finally, the conclusions are drawn in Section 4 based on the presented simulation results.

2 Implementation of MIMO-IOTA system with polyphase filters

An OFDM system can be efficiently implemented by fast fourier transform (FFT)/inverse fast fourier transform (IFFT) modules, whereas in an IOTA system extra filters are needed to do pulse shaping. A direct implementation of the IOTA system with finite impulse response filters on each sub-carrier will be highly complex and cause a long delay. As the duration of the prototype function can be very long, a large delay needs to be introduced to make the system causal and thus realisable.

The filter banks employed in multicarrier systems, like in [7–9], are designed to satisfy the perfect reconstruction (PR) condition under ideal channel setup, that is, no channel distortion is considered. However, the PR condition is difficult to achieve when the signal is passed through time-varying channels. As the wireless channel is doubly dispersive (hence time-varying) in nature and the PR property designed under perfect channel condition will no longer be PR under practical channel conditions, leading to a considerable amount of ISI/ICI. Therefore as long as the ISI/ICI can be reduced to a certain level according to the system requirements, it is not advisable to confine ourselves to the PR condition when designing a multicarrier system. Rather than deriving the implementation structure from filter bank theory as in [7–9], we propose to directly discretise the continuous time model and approximate the integration operation in the detector by corresponding Riemann sum, and our method will be described in details next.

The transmitted signal in a multicarrier system (including CP-based OFDM system and filter bank-based IOTA system) can be written in a general form as

$$s(t) = \sum_{n=-\infty}^{\infty} \sum_{m=0}^{N-1} a_{m,n} g_{m,n}(t) \tag{1}$$

where $a_{m,n}$ is the symbol modulated by the mth sub-carrier during the symbol time of index n, and $g_{m,n}(t)$ represents the synthesis basis, which is obtained by the time–frequency shifted version of the prototype function $g(t)$. In an OFDM system, the synthesis basis can be expressed as

$$g_{m,n}(t) = \begin{cases} \exp(\mathrm{j}2\pi mFt) & nT_0 - T_{\mathrm{cp}} \le t \le nT_0 + T \\ 0 & \text{otherwise} \end{cases} \tag{2}$$

where $F = 1/T$ is sub-carrier frequency spacing, T_{cp} is the length of CP, $T_0 = T + T_{\mathrm{cp}}$ is OFDM symbol duration and $a_{m,n}$ is a complex valued symbol.

For the IOTA system

$$g_{m,n}(t) = \exp(\mathrm{j}(m+n)\pi/2) \exp(\mathrm{j}2\pi m\nu_0 t) \\ g(t - n\tau_0), \quad \nu_0\tau_0 = 1/2 \tag{3}$$

where $g(t)$ is the well-designed pulse filter, such as EGF and IOTA pulses. In IOTA systems, the transmitted symbols are real-valued with symbol duration τ_0 and sub-carrier spacing ν_0. One can either set $\nu_0 = F$, $\tau_0 = T/2$ or $\nu_0 = F/2$, $\tau_0 = T$. Here, we adopt the former approach, that is, the sub-carrier spacing is kept the same as in OFDM, but symbol duration is reduced by half. In this case, the output

doi: 10.1049/iet-com.2012.0029

signal of the IOTA modulator can be expressed as

$$s(t) = \sum_{n=-\infty}^{\infty}\sum_{m=0}^{N-1}[a^{\mathrm{R}}_{m,n}g_{m,2n}(t) + a^{\mathrm{I}}_{m,n}g_{m,2n+1}(t)]$$
$$= \sum_{n=-\infty}^{\infty}\sum_{m=0}^{N-1}[a^{\mathrm{R}}_{m,n}g(t-2n\tau_0) + \mathrm{j}a^{\mathrm{I}}_{m,n}g(t-(2n+1)\tau_0)]$$
$$\times \exp(\mathrm{j}\pi(m+2n)/2)\exp(\mathrm{j}2\pi m v_0 t) \quad (4)$$

where $a^{\mathrm{R}}_{m,n}$ and $a^{\mathrm{I}}_{m,n}$ are the real and imaginary parts of the OQAM/OQPSK symbol $a_{m,n}$ conveyed by the sub-carrier of index m during the symbol time of index n. Note that in OQAM/OQPSK modulation, the I component $a^{\mathrm{R}}_{m,n}$ and Q components $a^{\mathrm{I}}_{m,n}$ are mis-aligned by half an OFDM symbol interval.

The demodulated signal at the m-sub-carrier and nth symbol can be expressed as

$$\hat{a}^{\mathrm{R}}_{m,n} = \mathrm{Re}\left\{\int s(t)g^*_{m,2n}(t)\mathrm{d}t\right\}$$
$$\hat{a}^{\mathrm{I}}_{m,n} = \mathrm{Re}\left\{\int s(t)g^*_{m,2n+1}(t)\mathrm{d}t\right\} \quad (5)$$

where $\mathrm{Re}(\cdot)$ denotes the real part of a complex variable.

By sampling $s(t)$ at rate $1/T_{\mathrm{s}}$ during time interval $[nT-\tau_0, nT+\tau_0)$, the transmitted signal can be written as

$$s(nT+kT_{\mathrm{s}}) = \sum_{l=-\infty}^{\infty}\sum_{m=0}^{N-1}[a^{\mathrm{R}}_{m,l}g(nT+kT_{\mathrm{s}}-lT)$$
$$+ \mathrm{j}a^{\mathrm{I}}_{m,l}g(nT+kT_{\mathrm{s}}-lT-T/2)]$$
$$\times \exp(\mathrm{j}\pi(m+2l)/2)\exp(\mathrm{j}2\pi mk/N) \quad (6)$$

where $k=-N/2, \ldots, N/2-1$. Denoting $s_k[n] = s[nN+k] = s(nT+kT_{\mathrm{s}})$, the above equation can be reformed as

$$s_k[n] = \sum_p g(pT+kT_{\mathrm{s}})$$
$$\left\{\sum_{m=0}^{N-1}a^{\mathrm{R}}_{m,n-p}\exp[\mathrm{j}\pi(m+2n-2p)/2]\exp[\mathrm{j}2\pi mk/N]\right\}$$
$$+ \sum_p g(pT+kT_{\mathrm{s}}-T/2)$$
$$\left\{\sum_{m=0}^{N-1}\mathrm{j}a^{\mathrm{I}}_{m,n-p}\exp[\mathrm{j}\pi(m+2n-2p)/2]\exp[\mathrm{j}2\pi mk/N]\right\}$$
$$= \sum_p\{g_k[p]A^k_N(a^{\mathrm{R}}_{m,n-p}) + g_{k-N/2}[p]A^k_N(\mathrm{j}a^{\mathrm{I}}_{m,n-p})\}$$
$$= g_k[n]\otimes A^k_N(a^{\mathrm{R}}_{m,n}) + g_{k-N/2}[n]\otimes A^k_N(\mathrm{j}a^{\mathrm{I}}_{m,n}) \quad (7)$$

where $\otimes$ denotes the convolution operation, and

$$A^k_N(x_{m,n}) = \sum_{m=0}^{N-1}x_{m,n}\exp(\mathrm{j}\pi(m+2n)/2)\exp(\mathrm{j}2\pi mk/N),$$
$$k=-N/2, \ldots, N/2-1 \quad (8)$$

$$g_k[n] = g[nN+k] = g(nT+kT_{\mathrm{s}}) \quad (9)$$

The structure of the IOTA transmitter is illustrated in the upper diagram of Fig. 1. According to the above analysis, the IOTA modulator in the transmitter can be easily implemented by an IFFT block defined in (8) followed by a bank of filters, which are obtained by partitioning the polyphase representation of $g(t)$ in the way defined in (9). Note that there are separate IFFT chains for the I and Q components, which are combined after polyphase filtering. The phase correction ($j^{(m+2n)}$ for the I channel and $j^{(m+2n+1)}$ for the Q channel) before the IFFT operation is because of the first exponential term in (8). An $N/2$ rotation of IFFT output is needed here to shift the zero frequency sub-carrier to middle position.

At the receiver, we sample the received signal $r(t)$ at rate $1/T_{\mathrm{s}}$ (5) can be reformed as

$$\hat{a}^{\mathrm{R}}_{m,n} = \mathrm{Re}\left\{\int s(t)g^*_{m,2n}(t)\mathrm{d}t\right\} \simeq$$
$$\left\{T_{\mathrm{s}}\sum_{l=-\infty}^{\infty}\sum_{k=-N/2}^{N/2-1}r(lT+kT_{\mathrm{s}})g^*_{m,2n}(lT+kT_{\mathrm{s}})\right\}$$
$$= \mathrm{Re}\left\{T_{\mathrm{s}}\exp[-\mathrm{j}\pi((m+2n)/2]\sum_{k=-N/2}^{N/2-1}\right.$$
$$\left.\sum_{l=-\infty}^{\infty}r_k[l]g_k[l-n]\exp[-\mathrm{j}2\pi mk/N]\right\}$$
$$= \mathrm{Re}\left\{T_{\mathrm{s}}\exp[-\mathrm{j}\pi((m+2n)/2]\sum_{k=-N/2}^{N/2-1}\right.$$
$$\left.r_k[n]\otimes g_k[-n]\exp[-\mathrm{j}2\pi mk/N]\right\}$$
$$= \mathrm{Re}\left\{T_{\mathrm{s}}j^{(m-2n)}\sum_{k=-N/2}^{N/2-1}r_k[n]\otimes g_k[-n]\right.$$
$$\left.\exp(-\mathrm{j}2\pi m(k+N/2)/N\right\} \quad (10)$$

Similarly, we can obtain

$$\hat{a}^{\mathrm{I}}_{m,n} = \mathrm{Re}\left\{\int s(t)g^*_{m,2n+1}(t)\mathrm{d}t\right\} \simeq$$
$$\left\{T_{\mathrm{s}}j^{-(m+2n)}\sum_{k=0}^{N-1}r_k[n]\otimes g_{k-N/2}[-n]\exp(-\mathrm{j}2\pi mk/N\right\} \quad (11)$$

where

$$g_k[-n] = g[-nN+k] = g(-NT+kT_{\mathrm{s}})$$

Note that the approximation in (10) and (11) is because of the fact that the Riemann sum can be made as close as desired to the original integral inside the $\mathrm{Re}\{\cdot\}$ operator by reducing the interval T_{s} (i.e. by increasing N for a fixed symbol duration T), as long as the original integral itself is integrable. Therefore the approximation only incurs minor distortion as long as the system parameters (FFT size N and sub-carrier frequency spacing $1/T$) are carefully designed. A more detailed examination of the approximation accuracy under

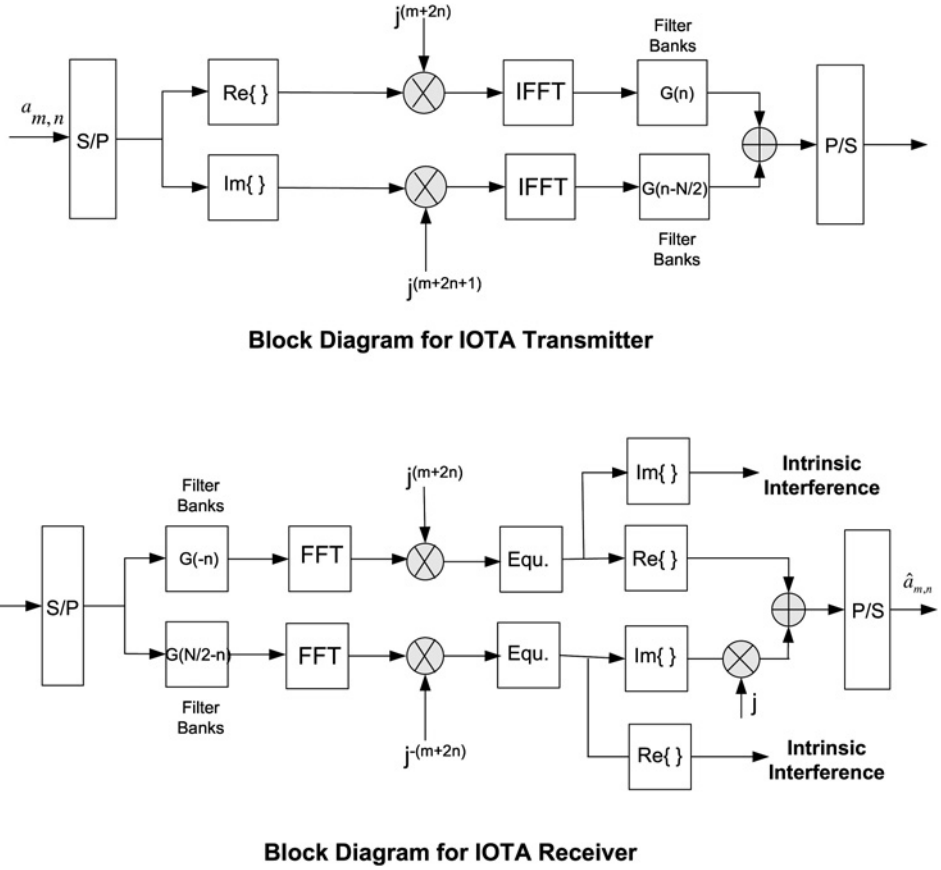

Fig. 1 *Block diagrams for IOTA transmitter and receiver*

ideal channel condition with different pulse shapes can be found in [19].

According to (10) and (11), the IOTA demodulator can be implemented by filter banks $g_k[n]$ and $g_{k-N/2}[n]$ followed by an FFT block, as shown in the lower diagram of Fig. 1. The pulse filtering is implemented efficiently using polyphase filter banks $G(n)$ and $G(n-N/2)$. Like in the transmitter, the FFT operations are conducted separately for the I and Q components of OQAM symbols. The real part of the equalised and phase corrected signal from the I channel is combined with the imaginary part of the equalised and phase-corrected signal from the Q channel, based on which the transmitted symbols can be detected. As indicated by Fig. 1, the imaginary part of the equalised and phase corrected signal from the I channel and the real part of the equalised and phase corrected signal from the Q channel are regarded as intrinsic interference and not used for data detection.

The implementation of MIMO-IOTA is based on the transmitter and receiver structure depicted in Fig. 1, which only shows an uncoded single-input, single-output (SISO)-IOTA system. In MIMO-IOTA transmitter, several parallel chains of the SISO-IOTA transmitter is utilised, one for each transmitting antenna. The MIMO-IOTA receiver, however, needs to be modified to facilitate efficient channel

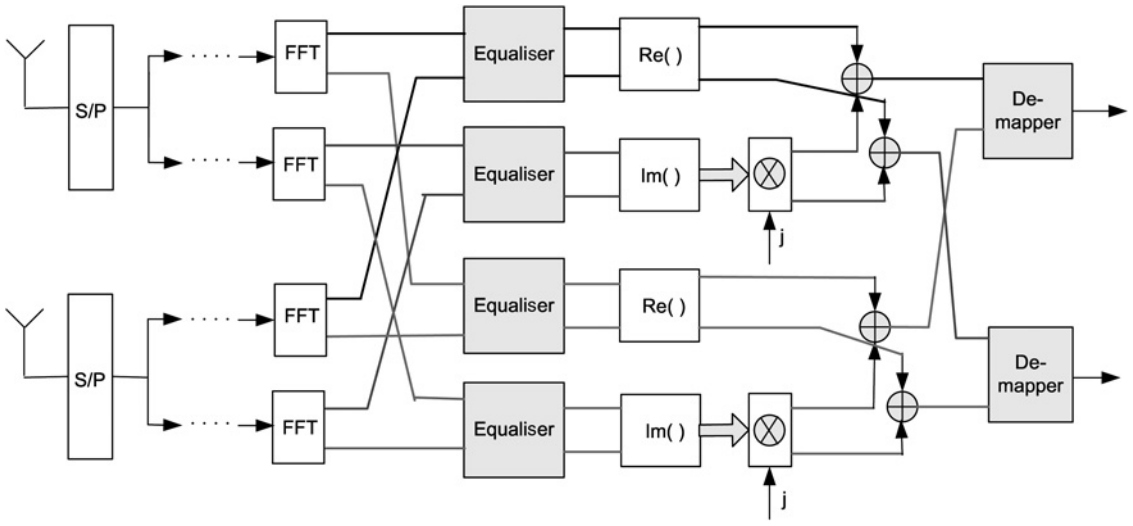

Fig. 2 *Sub-carrier mapping and demapping in MIMO-IOTA*

doi: 10.1049/iet-com.2012.0029

estimation and equalisation. In MIMO-IOTA receiver, equalisation is performed on per-sub-carrier basis, that is, symbols corresponding to the same sub-carrier at different antennas are jointly equalised. This necessitates the signal mapping between FFT block and the equaliser as well as the demapper (demodulator). The mapping and demapping processes are elaborated in Fig. 2 using $N = 2$ sub-carriers and $N_r = 2$ receive antennas system as an example. For simplicity, the filter banks and phase correction are omitted in the figure. A soft demapper (demodulator) is applied to the output of equaliser to derive soft estimate of the transmitted bits, which serve as inputs for the channel decoder to facilitate soft-input decoding.

Note that the proposed MIMO-IOTA implementation can be easily integrated into OFDM-based systems as they share many functional blocks. The separation of real and imaginary branches in IOTA implementation facilitates parallel processing and functional block sharing at the cost of increased memory and processing delay. The complexity of the IOTA transmitter can be further decreased by utilising the special structure of the input to IFFT blocks: the input symbol in the I branch onto the mth sub-carrier of the IFFT is either purely real-valued (for even m) or purely imaginary-valued (for odd m) all the time, and it is the other way around for the Q branch. Such special input structure to IFFT block can be utilised to greatly reduce the computation complexity based on the two-way machine-specific single-instruction, multiple-data instructions as explained in [20].

In Figs. 3 and 4, we compare a coded MIMO-IOTA system with a coded MIMO-OFDM system. The structure of the coded MIMO-IOTA system is similar to the one shown in Fig. 5, but without precoding and blind channel estimation. For MIMO-OFDM, we use QPSK/16-QAM modulation, the length of CP is 0.8 μs. For MIMO-IOTA, we use OQPSK/16-OQAM modulation, and the number of filter taps for each sub-carrier is 6. In our experiments, we use the following channel model adopted by the IEEE 802.11 working group [21]

$$\begin{aligned} h_k &= \mathcal{N}(0, 0.5\sigma_k^2) + \mathrm{j}\mathcal{N}(0, 0.5\sigma_k^2) \\ \sigma_k^2 &= \sigma_0^2 \exp(-kT_s/T_{\mathrm{RMS}}) \\ \sigma_0^2 &= 1 - \exp(-T_s/T_{\mathrm{RMS}}) \end{aligned} \tag{12}$$

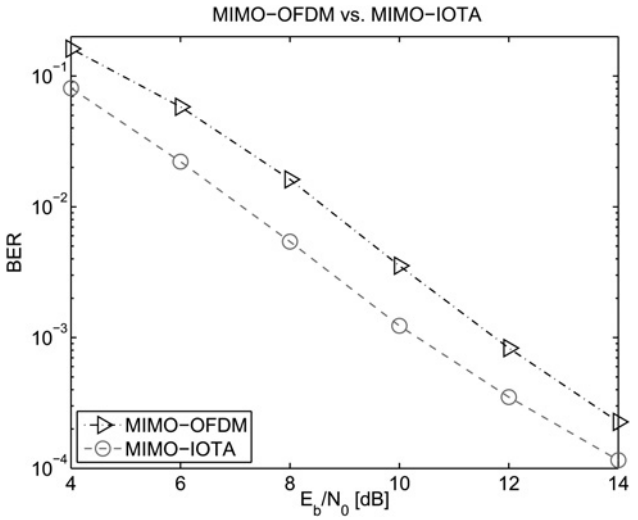

Fig. 3 *Performance comparison between OQPSK-modulated MIMO-IOTA and QPSK modulated MIMO-OFDM*

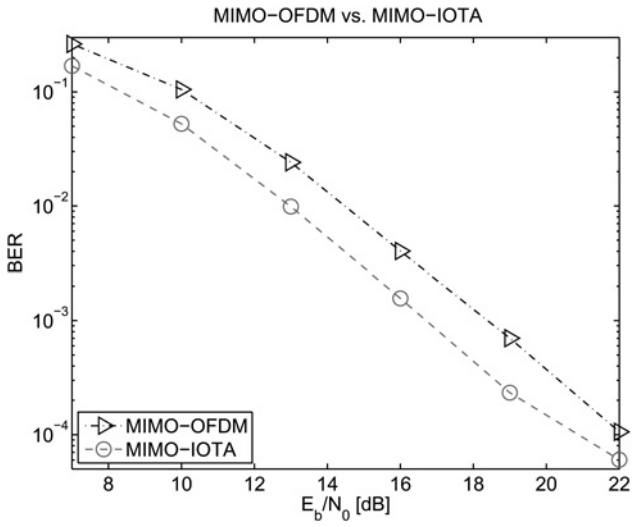

Fig. 4 *Performance comparison between 16-OQAM-modulated MIMO-IOTA and 16-QAM modulated MIMO-OFDM*

where $\mathcal{N}(\mu, \sigma^2)$ denotes the normal distribution with mean value μ and variance σ^2, h_k is the complex channel gain of the kth tap, T_{RMS} is the RMS delay spread of the channel, T_s is the sampling period and σ_0^2 is chosen so that the condition $\sum_k \sigma_k^2 = 1$ is satisfied to ensure same average received power. The number of samples to be taken in the impulse response should ensure sufficient decay of the impulse response tail, for example, $k_{\max} = 10 \times T_{\mathrm{RMS}}/T_s$. The simulation parameters, which are common for both IOTA and OFDM are summarised in Table 1.

As indicated by Fig. 3, the OQPSK modulated MIMO-IOTA system yields a performance gain of 1 dB over the QPSK modulated MIMO-OFDM system. Compared with OFDM, IOTA achieves improved power efficiency (better error rate performance) and spectral efficiency (elimination of CP). The similar conclusion can be drawn for Fig. 4, where we show the performance comparison between the 16-OQAM modulated MIMO-IOTA system and 16-QAM modulated MIMO-OFDM system.

3 Blind channel estimation and data detection for linearly precoded MIMO-IOTA system

In this section, we introduce blind channel estimation schemes for linearly precoded IOTA systems. To ease understanding, we start with an analysis of single antenna IOTA system and see how the signal can be recovered given the knowledge of the channel. Then we extend our analysis to MIMO-IOTA system and describe our proposed blind channel estimation algorithm.

Recall that the signal at the input of IOTA modulator can be expressed in the following general form as

$$s(t) = \sum_{n=-\infty}^{\infty} \sum_{m=0}^{N-1} a_{m,n} g_{m,n}(t)$$

where $g_{m,n}(t)$ is the shifted version of $g(t)$ in time and frequency, and $a_{m,n}(t)$ is real-valued symbol, can be either $a_{m,n}^{\mathrm{R}}(t)$ or $a_{m,n}^{\mathrm{I}}(t)$ in (4). Owing to the real-orthogonality condition on the prototype function $g(t)$, we have [16]

$$\mathrm{Re}\{g_{m,n}(t) g_{m_0,n_0}^*(t)\} = \delta_{m,m_0} \delta_{n,n_0} \tag{13}$$

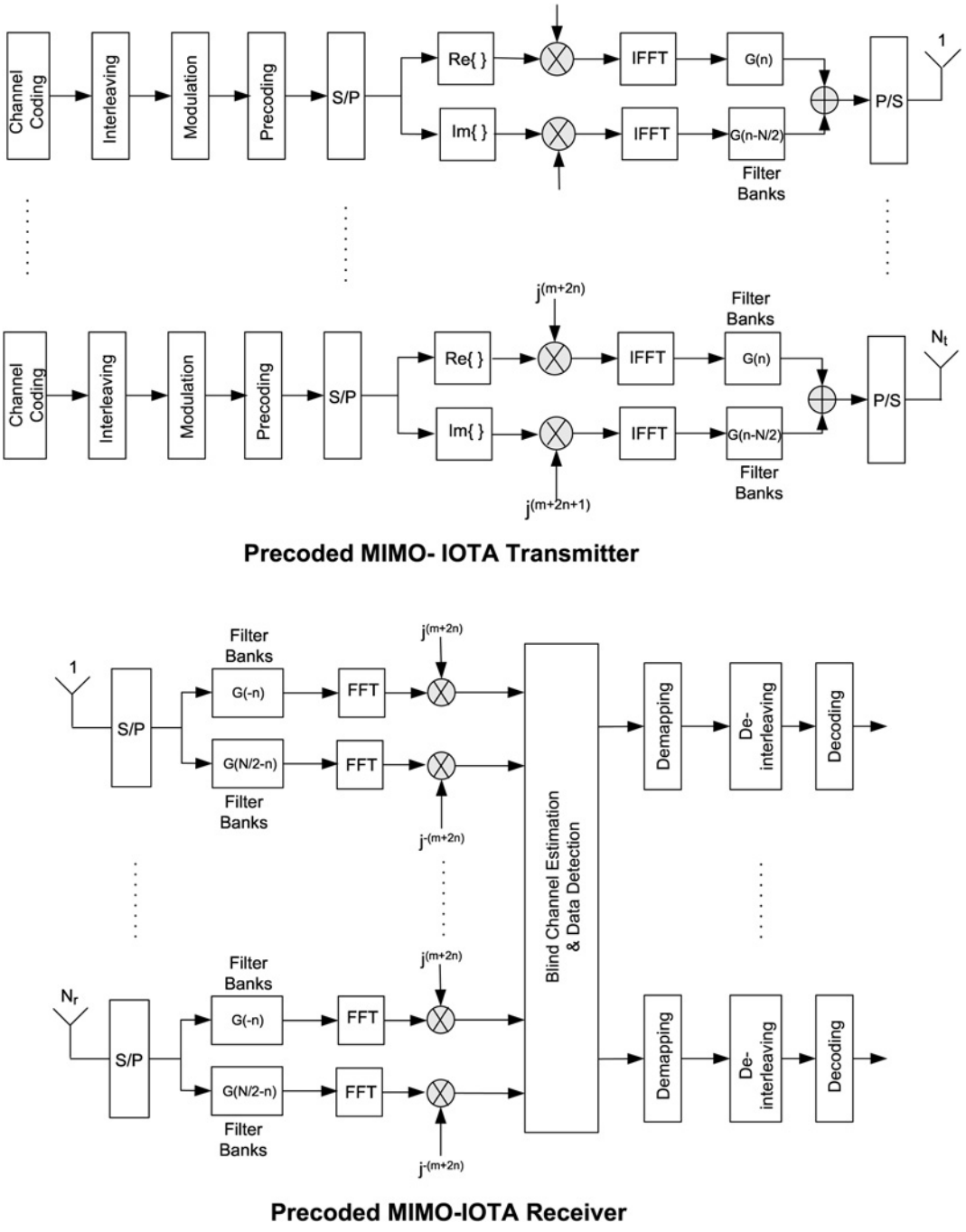

Fig. 5 *Block diagrams for precoded MIMO-IOTA transmitter and receiver*

In the absence of fading and noise, the demodulated symbol corresponding to the mth sub-carrier and the nth symbol can be expressed as

$$\hat{a}_{m,n} = \int s(t) g^*_{m,n}(t)\mathrm{d}t = a_{m,n} + \underbrace{\sum_{(m\prime,n\prime)\neq(m,n)} a_{m\prime,n\prime} \int g_{m\prime,n\prime}(t) g^*_{m,n}(t)\mathrm{d}t}_{A^{(\mathrm{i})}_{m,n}} \quad (14)$$

According to (13), the intrinsic interference $A^{(\mathrm{i})}_{m,n} = \mathrm{j}a^{(\mathrm{i})}_{m,n}$ in (14) is purely imaginary. Thus, we can perfectly recover the transmitted symbol by simply taking the real part of the demodulation output $\hat{a}_{m,n}$.

In the presence of fading and noise, the received signal becomes

$$s(t) = \sum_{n=-\infty}^{\infty} \sum_{m=0}^{N-1} H_{m,n} a_{m,n} g_{m,n}(t) + n(t)$$

where $H_{m,n}$ denotes the channel response at the mth sub-carrier during the nth symbol period. In this case, the demodulated symbol becomes

$$\hat{a}_{m,n} = \int s(t) g^*_{m,n}(t)\mathrm{d}t = H_{m,n} a_{m,n} + \underbrace{\sum_{(m\prime,n\prime)\neq(m,n)} H_{m\prime,n\prime} a_{m\prime,n\prime} \int g_{m\prime,n\prime}(t) g^*_{m,n}(t)\mathrm{d}t}_{I_{m,n}} + n_{m,n} \quad (15)$$

doi: 10.1049/iet-com.2012.0029

Table 1 Simulation parameters

Channel model	IEEE 802.11a
system bandwidth	20 MHz
carrier frequency	5 GHz
FFT size	$N = 64$
OFDM symbol duration	3.2 μs
length of CP for OFDM	0.8 μs
correlation window length	$N_{\text{win}} = 32$
T_{RMS}	50 ns
sampling frequency	20 MHz
polynomial of convolutional code	$(133\ 171)_8$
interleaver	random interleaver of size 256
equaliser type	MMSE
number of transmit antennas	$N_t = 2$
number of receive antennas	$N_r = 2$

As the prototype function $g(t)$ is chosen to be well localised both in time and frequency, the intrinsic interference $I_{m,n}$ in (15) only depends on a restricted set of time–frequency positions (m', n') around the symbol of interest. Assuming that the channel remains relatively constant at those positions, that is, $H_{m,n}^{m',n'} \approx H_{m,n}$, the intrinsic interference $I_{m,n}$ can be approximated as [16]

$$I_{m,n} \simeq H_{m,n} \underbrace{\sum_{(m',n')\neq(m,n)} a_{m',n'} \int g_{m',n'}(t) g_{m,n}^{*}(t)\,\mathrm{d}t}_{\mathrm{j}a_{m,n}^{(\mathrm{i})}} = H_{m,n}\mathrm{j}a_{m,n}^{(\mathrm{i})} \tag{16}$$

Combining (15) and (16) yields

$$\hat{a}_{m,n} \simeq H_{m,n}[a_{m,n} + \mathrm{j}a_{m,n}^{(\mathrm{i})}] + n_{m,n} \tag{17}$$

With the system model shown in Fig. 1, the input to the first and the second equaliser at the IOTA receiver can be expressed as

$$\begin{aligned} y_{m,n}^{\mathrm{R}} &= H_{m,n}[a_{m,n}^{\mathrm{R}} + \mathrm{j}a_{m,n}^{(\mathrm{i})}] + n_{m,n}^{\mathrm{R}} \\ y_{m,n}^{\mathrm{I}} &= H_{m,n}[a_{m,n}^{(\mathrm{r})} + \mathrm{j}a_{m,n}^{\mathrm{I}}] + n_{m,n}^{\mathrm{I}} \end{aligned} \tag{18}$$

where $a_{m,n}^{(\mathrm{i})}$ and $a_{m,n}^{(\mathrm{r})}$ are the intrinsic interference for the first and second FFT chains, respectively. Given the knowledge of the channel coefficient $H_{m,n}$, the transmitted OQPSK/OQAM symbol $a_{m,n}$ can be recovered by ZF equalisation, that is

$$\begin{aligned} \hat{a}_{m,n} &= \mathrm{Re}\{y_{m,n}^{\mathrm{R}}/H_{m,n}\} + \mathrm{j}\{y_{m,n}^{\mathrm{I}}/H_{m,n}\} \\ &= a_{m,n}^{\mathrm{R}} + \mathrm{j}a_{m,n}^{\mathrm{I}} + \{n_{m,n}^{\mathrm{R}}/H_{m,n}\} + \{n_{m,n}^{\mathrm{I}}/H_{m,n}\} \\ &= a_{m,n} + v_{m,n} \end{aligned} \tag{19}$$

where $v_{m,n}$ is the combined noise term. An MMSE equalisation can be designed similarly.

Next we discuss how the channel frequency response $H_{m,n}$ $(m = 1, \ldots, N;\ n = 1, \ldots, B)$ can be estimated without pilot symbols.

Fig. 5 shows the linear precoded MIMO-IOTA system with N_t transmit antennas and N_r receive antennas. Denote $\boldsymbol{d}_i \in \mathbb{C}^{N\times 1}$ as the kth block of data stream transmitted by the ith transmit antenna, where N is the number of sub-carriers (FFT size). Each block of data goes through linear precoding, resulting in

$$\boldsymbol{a}_i = \boldsymbol{A}\boldsymbol{d}_i = \boldsymbol{a}_i^{\mathrm{R}} + \mathrm{j}\boldsymbol{a}_i^{\mathrm{I}} \in \mathbb{C}^{N\times 1}$$

where $\boldsymbol{A}$ is the precoding matrix. The real and imaginary parts of the precoded data $\boldsymbol{a}_i^{\mathrm{R}}$ and $\boldsymbol{a}_i^{\mathrm{I}}$ are processed by separate IFFT chains and bank of filters, then transmitted from each transmit antenna. Note that we have left out the symbol index k to simplify notation whenever no ambiguity arises.

Denote the impulse response of a L-path channel between the ith transmit antenna and the jth receive antenna as $h_{ji}[l]$, $l = 0, \ldots, L-1$. The frequency-domain channel response for each transmit–receive antenna pair is defined as

$$\boldsymbol{H}_{ji} = \begin{bmatrix} H_{ji}[0] & H_{ji}[1] & \cdots & H_{ji}[N-1] \end{bmatrix}^{\mathcal{T}} \in \mathbb{C}^{N\times 1}$$

where

$$H_{ji}[m] = \sum_{l=0}^{\mathrm{L}} h_{ji}[l] \exp(-\mathrm{j}2\pi ml/N)$$

According to (18), the output of IOTA demodulator at the jth receive antenna at can be expressed as

$$\boldsymbol{y}_j^{\mathrm{R}} = \sum_{i=1}^{N_t} \mathrm{diag}\{H_{ji}\}[\boldsymbol{a}_i^{\mathrm{R}} + \mathrm{j}\boldsymbol{a}_i^{(\mathrm{i})}] + \boldsymbol{n}_j^{\mathrm{R}}$$

$$\boldsymbol{y}_j^{\mathrm{I}} = \sum_{i=1}^{N_t} \mathrm{diag}\{H_{ji}\}[\boldsymbol{a}_i^{(\mathrm{r})} + \mathrm{j}\boldsymbol{a}_i^{\mathrm{I}}] + \boldsymbol{n}_j^{\mathrm{I}}$$

where $\boldsymbol{n}_j^{\mathrm{R}}$ and $\boldsymbol{n}_j^{\mathrm{I}}$ are zero mean white Gaussian noise vectors with covariance matrix $((N_0)/(2))\boldsymbol{I}$.

The auto-correlation matrix of the received signal can be derived as

$$\begin{aligned} \boldsymbol{R}_{jj} &= \mathrm{E}[\boldsymbol{y}_j^{\mathrm{R}}(\boldsymbol{y}_j^{\mathrm{R}})^{\mathcal{H}} + \boldsymbol{y}_j^{\mathrm{I}}(\boldsymbol{y}_j^{\mathrm{I}})^{\mathcal{H}}] \\ &= \mathrm{E}\left[\left(\sum_{i=1}^{N_t} \mathrm{diag}\{H_{ji}\}[\boldsymbol{a}_i^{\mathrm{R}} + \mathrm{j}\boldsymbol{a}_i^{(\mathrm{i})}] + \boldsymbol{n}_j^{\mathrm{R}}\right) \left(\sum_{i=1}^{N_t} \mathrm{diag}\{H_{ji}\}[\boldsymbol{a}_i^{\mathrm{R}} + \mathrm{j}\boldsymbol{a}_i^{(\mathrm{i})}] + \boldsymbol{n}_j^{\mathrm{R}}\right)^{\mathcal{H}}\right] \\ &\quad + \mathrm{E}\left[\left(\sum_{i=1}^{N_t} \mathrm{diag}\{H_{ji}\}[\boldsymbol{a}_i^{(\mathrm{r})} + \mathrm{j}\boldsymbol{a}_i^{\mathrm{I}}] + \boldsymbol{n}_j^{\mathrm{I}}\right) \left(\sum_{i=1}^{N_t} \mathrm{diag}\{H_{ji}\}[\boldsymbol{a}_i^{(\mathrm{r})} + \mathrm{j}\boldsymbol{a}_i^{\mathrm{I}}] + \boldsymbol{n}_j^{\mathrm{I}}\right)^{\mathcal{H}}\right] \\ &\simeq \sum_{i=1}^{N_t} \mathrm{diag}\{H_{ji}\}\boldsymbol{A}\boldsymbol{A}^{\mathcal{H}}\mathrm{diag}\{H_{ji}\}^{\mathcal{H}} + N_0\boldsymbol{I} \qquad (20) \\ &= \sum_{i=1}^{N_t} (\boldsymbol{H}_{ji}\boldsymbol{H}_{ji}^{\mathcal{H}}) \odot (\boldsymbol{A}\boldsymbol{A}^{\mathcal{H}}) + N_0\boldsymbol{I} \qquad (21) \end{aligned}$$

where $\odot$ denotes element-by-element multiplication.

Note that the intrinsic interference is omitted in (20), therefore it is an approximation rather than an equality. Equation (21) holds since $\boldsymbol{a}_i = \boldsymbol{A}\boldsymbol{d}_i = \boldsymbol{a}_i^{\mathrm{R}} + \mathrm{j}\boldsymbol{a}_i^{\mathrm{I}}$

and $\mathrm{E}[\boldsymbol{d}_i\boldsymbol{d}_i^{\mathcal{H}}] = \boldsymbol{I}$. If the matrix $\boldsymbol{A}\boldsymbol{A}^{\mathcal{H}}$ has unit diagonal entries and non-zero off-diagonal entries, which can always be satisfied with proper choice of $\boldsymbol{A}$, we can perform an element-by-element division of $\boldsymbol{R}_{jj}$ to obtain

$$\boldsymbol{W}_{jj} = \boldsymbol{R}_{jj}./(\boldsymbol{A}\boldsymbol{A}^{\mathcal{H}}) = \sum_{i=1}^{N_\mathrm{t}} (\boldsymbol{H}_{ji}\boldsymbol{H}_{ji}^{\mathcal{H}}) + N_0\boldsymbol{I} \in \mathbb{C}^{N\times N} \quad (22)$$

where ./ denotes element-by-element division. Let us define

$$\boldsymbol{H}_j = \left[\boldsymbol{H}_{j1}\,\boldsymbol{H}_{j2}\ldots\boldsymbol{H}_{jN_\mathrm{t}}\right] \in \mathbb{C}^{N\times N_\mathrm{t}}$$

Equation (22) can be reformed as

$$\boldsymbol{W}_{jj} = \boldsymbol{H}_j\boldsymbol{H}_j^{\mathcal{H}} + N_0\boldsymbol{I}$$

Assume $\boldsymbol{H}_j$ has full column rank, performing the singular value decomposition of $\boldsymbol{W}_{jj}$ yields $\boldsymbol{W}_{jj} = \boldsymbol{U}_j\boldsymbol{\Lambda}_j\boldsymbol{V}_j^{\mathcal{H}}$. Then the channel $\boldsymbol{H}_j$ can be estimated as

$$\hat{\boldsymbol{H}}_j = \boldsymbol{U}_j\boldsymbol{\Lambda}_j^{1/2} = \boldsymbol{H}_j\boldsymbol{Q}_j \quad (23)$$

where $\hat{\boldsymbol{H}}_j$ is an estimate of $\boldsymbol{H}_j$, and $\boldsymbol{Q}_j$ is an unitary ambiguity matrix.

After $\boldsymbol{H}_j$ is estimated, an estimate of channel $\boldsymbol{H}_k$, $k \neq j$ can be derived from the cross-correlation of the signals received at kth and the jth antennas

$$\begin{aligned}\boldsymbol{R}_{kj} &= \mathrm{E}[\boldsymbol{y}_k^{\mathrm{R}}(\boldsymbol{y}_j^{\mathrm{R}})^{\mathcal{H}} + \boldsymbol{y}_k^{\mathrm{I}}(\boldsymbol{y}_j^{\mathrm{I}})^{\mathcal{H}}]\\ &= \mathrm{E}\left[\left(\sum_{i=1}^{N_\mathrm{t}}\mathrm{diag}\{H_{ki}\}[\boldsymbol{a}_i^{\mathrm{R}} + \mathrm{j}\boldsymbol{a}_i^{(\mathrm{i})}] + \boldsymbol{n}_k^{\mathrm{R}}\right)\right.\\ &\quad\left.\left(\sum_{i=1}^{N_\mathrm{t}}\mathrm{diag}\{H_{ji}\}[\boldsymbol{a}_i^{\mathrm{R}} + \mathrm{j}\boldsymbol{a}_i^{(\mathrm{i})}] + \boldsymbol{n}_j^{\mathrm{R}}\right)^{\mathcal{H}}\right]\\ &\quad + \mathrm{E}\left[\left(\sum_{i=1}^{N_\mathrm{t}}\mathrm{diag}\{H_{ki}\}[\boldsymbol{a}_i^{(\mathrm{r})} + \mathrm{j}\boldsymbol{a}_i^{\mathrm{I}}] + \boldsymbol{n}_k^{\mathrm{I}}\right)\right.\\ &\quad\left.\left(\sum_{i=1}^{N_\mathrm{t}}\mathrm{diag}\{H_{ji}\}[\boldsymbol{a}_i^{(\mathrm{r})} + \mathrm{j}\boldsymbol{a}_i^{\mathrm{I}}] + \boldsymbol{n}_j^{\mathrm{I}}\right)^{\mathcal{H}}\right]\\ &\simeq \sum_{i=1}^{N_\mathrm{t}}\mathrm{diag}\{H_{ki}\}\boldsymbol{A}\boldsymbol{A}^{\mathcal{H}}\mathrm{diag}\{H_{ji}\}^{\mathcal{H}} = \sum_{i=1}^{N_\mathrm{t}}(\boldsymbol{H}_{ki}\boldsymbol{H}_{ji}^{\mathcal{H}})\odot(\boldsymbol{A}\boldsymbol{A}^{\mathcal{H}}) \quad (24)\end{aligned}$$

Performing element-wise division of $\boldsymbol{R}_{kj}$ by $\boldsymbol{A}\boldsymbol{A}^{\mathcal{H}}$, yields

$$\boldsymbol{W}_{kj} = \boldsymbol{R}_{kj}./(\boldsymbol{A}\boldsymbol{A}^{\mathcal{H}}) = \sum_{i=1}^{N_\mathrm{t}}(\boldsymbol{H}_{ki}\boldsymbol{H}_{ji}^{\mathcal{H}}) = \boldsymbol{H}_k\boldsymbol{H}_j^{\mathcal{H}} \quad (25)$$

Based on (25), an estimate of $\boldsymbol{H}_k$ can be derived as

$$\hat{\boldsymbol{H}}_k = \boldsymbol{W}_{kj}(\hat{\boldsymbol{H}}_j^{\mathcal{H}})^{\dagger} = \boldsymbol{H}_k\boldsymbol{H}_j^{\mathcal{H}}(\boldsymbol{H}_j\mathbf{Q}_j)^{\dagger} = \boldsymbol{H}_k\boldsymbol{Q}_j \quad (26)$$

where † denotes the pseudo-inverse, and $\hat{\boldsymbol{H}}_j$ is an estimate of $\boldsymbol{H}_j$ given in (23). By repeating the above process to all the remaining receive antennas, the channel matrices can be estimated up to the same unitary ambiguity matrix $\boldsymbol{Q}_j$.

Now we show how the unitary ambiguity matrix $\boldsymbol{Q}_j$ can be identified by using just one pilot placed at the pth sub-carrier. After the IOTA demodulation, the received signal at the pilot sub-carrier can be expressed as

$$\boldsymbol{Y}_p = \boldsymbol{H}_p\boldsymbol{T}_p + \boldsymbol{N}_p \in \mathbb{C}^{N_\mathrm{r}\times B} \quad (27)$$

where $\boldsymbol{H}_p \in \mathbb{C}^{N_r\times N_t}$ is the channel matrix corresponding to the pth sub-carrier between N_t transmit antennas and N_r receive antennas. $\boldsymbol{Y}_p$ and $\boldsymbol{N}_p$ denotes the received signal and noise matrices, respectively. The pilot matrix $\boldsymbol{T}_p \in \mathbb{C}^{N_t\times B}$ is defined as

$$\boldsymbol{T}_p = \begin{bmatrix} t_1(p,1) & t_1(p,2) & \ldots & t_1(p,B)\\ \vdots & \ddots & \ddots & \vdots\\ t_{N_\mathrm{t}}(p,1) & t_{N_\mathrm{t}}(p,2) & \ldots & t_{N_\mathrm{t}}(p,B)\end{bmatrix}$$

where B is the number of data blocks, $t_m(p, n)$ is the pilot symbol transmitted from the mth transmit antenna and inserted at the pth sub-carrier of the nth data block.

Based on (27), the pilot channel can be estimated as

$$\tilde{\boldsymbol{H}}_p = \boldsymbol{Y}_p\boldsymbol{T}_p^{\dagger}$$

As $\hat{\boldsymbol{H}}_p = \tilde{\boldsymbol{H}}_p\boldsymbol{Q}_j$, where $\hat{\boldsymbol{H}}_p$ is the estimated pilot channel derived from the above procedure shown in (21)–(26), the unitary ambiguity matrix $\boldsymbol{Q}_j$ can thus be identified as

$$\boldsymbol{Q}_j = \tilde{\boldsymbol{H}}_p^{-1}\hat{\boldsymbol{H}}_p = [\boldsymbol{Y}_p\boldsymbol{T}_p^{\dagger}]^{-1}\hat{\boldsymbol{H}}_p$$

Once the channel has been estimated, coherent data detection can be carried out using the estimated channel.

The simulation results of the proposed blind channel estimation and data detection for the linear precoded MIMO-IOTA system are shown in Figs. 6 and 7. Performance comparison is also made between IOTA and OFDM systems. We use the IEEE 802.11 WLAN channel model with 11 sample-spaced multipaths. The FFT size is 64. The employed convolutional codes has a rate of 1/2, constraint length of 7 and generator polynomial $(133,171)_8$. The number of antennas is 2 for both transmitter and receiver. For MIMO-OFDM, we use QPSK modulation, the length of CP is 16. For MIMO-IOTA, we use OQPSK modulation, number of filter taps each sub-carrier is 6. For linear precoding, we adopt the circulant precoding matrix from [22] (see (28))

where $0 < p < 1$. With the precoding matrix $\boldsymbol{A}$ specified in

$$\boldsymbol{A} = \begin{bmatrix} \sqrt{p} & \sqrt{1-pN-1} & \ldots & \sqrt{1-pN-1}\\ \sqrt{1-pN-1} & \sqrt{p} & \ldots & \sqrt{1-pN-1}\\ \vdots & \vdots & \ddots & \vdots\\ \sqrt{1-pN-1} & \ldots & \sqrt{1-pN-1} & \sqrt{p}\end{bmatrix} \quad (28)$$

doi: 10.1049/iet-com.2012.0029

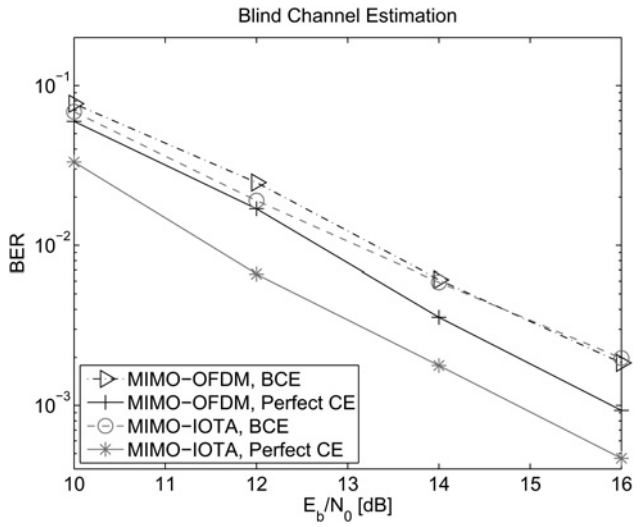

Fig. 6 *Performance of blind channel estimation and data detection for linearly precoded MIMO-IOTA and MIMO-OFDM*

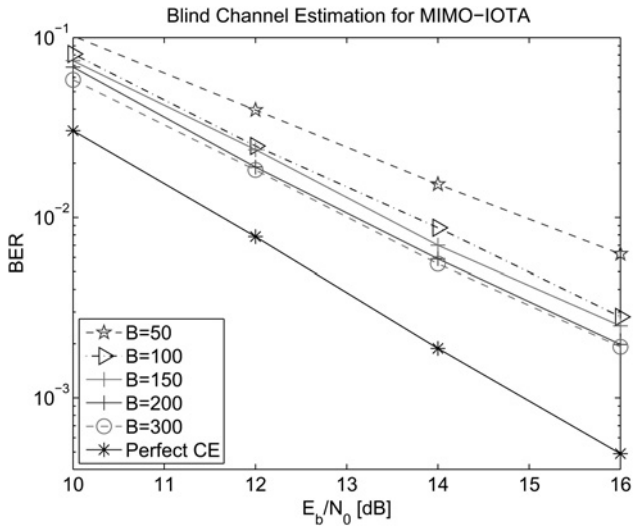

Fig. 7 *Performance of blind channel estimation and data detection for linearly precoded MIMO-IOTA*

(28), $\boldsymbol{A}\boldsymbol{A}^{\mathcal{H}}$ can be obtained as

$$\boldsymbol{A}\boldsymbol{A}^{\mathcal{H}} = \begin{bmatrix} 1 & \alpha & \dots & \alpha \\ \alpha & 1 & \alpha & \alpha \\ \vdots & \vdots & \ddots & \vdots \\ \alpha & \dots & \alpha & 1 \end{bmatrix} \tag{29}$$

which satisfies the conditions that it has unit diagonal elements and non-zero off-diagonal elements. The off-diagonal element α can be adjusted by changing p in the precoding matrix $\boldsymbol{A}$. In our experiments, we set the value of p to 0.5.

Fig. 6 shows that the proposed blind channel estimation and data detection scheme for MIMO-IOTA performs better than that of the MIMO-OFDM system at low-to-medium SNRs, however, their performance converge at high SNR. In this experiment, we assume the channel remains relatively static during the transmission of $B = 200$ data blocks. The performance loss in the IOTA system is because of the intrinsic interference, which causes imperfect estimate of the auto-correlation and cross-correlation matrices expressed by (21) and (24). Although the IOTA system does not show much improved power efficiency compared with OFDM in this case, it is still a preferred solution since it improves the spectral efficiency by 20% as a result of the elimination of CP.

One can also see from Fig. 6 that given perfect channel estimation, the MIMO-IOTA system outperforms MIMO-OFDM by 1 dB, which concurs with the experimental results shown in the previous section. This means the IOTA system has better potential to improve power efficiency once the intrinsic interference is mitigated.

Fig. 7 shows the performance of blind channel estimation for the MIMO-IOTA system when the data block size changes from $B = 50$ to 300. Apparently, the performance improves as the block size increases since the auto-correlation and cross-correlation matrices can be more accurately estimated. One can also observe that the convergence can be reached with relatively short block size, the performance becomes saturated when B goes beyond 200. This is a desired feature since shorter block size means smaller detection latency in data detection process.

4 Conclusions

In this paper, we investigate the design of IOTA multicarrier systems with an aim to improve the power and spectral efficiencies of a wireless communication system. First, we presented a polyphase implementation of the MIMO-IOTA system. Results show that in addition to the improved spectral efficiency because of the elimination of CP, the proposed MIMO-IOTA system also achieves improved power efficiency. We proposed a linearly precoded IOTA system in order to facilitate blind channel estimation so that both CP and training sequences can be avoided, resulting in a multicarrier system with a much higher spectral efficiency than conventional OFDM systems considering that the overhead imposed by training data and CP can be up to 50% for fast-fading channels. Our results show that the proposed blind channel estimation scheme reaches convergence with relatively small block size, hence short detection latency in data detection process. It achieves better performance compared with the OFDM system at low to medium SNRs, and comparable performance at high SNRs. The IOTA system is also shown to have better potential to improve power efficiency compared with the OFDM system. How to mitigate the intrinsic interference in IOTA in order to exploit its potential will be the future research topic for the authors.

5 Acknowledgments

This work was sponsored by the UK Engineering and Physical Sciences Research Council (EPSRC) under grant number EP/JO17655/1. The authors would like to acknowledge its financial support.

6 References

1 Bingham, J.: 'Multicarrier modulation for data transmission: an idea whose time has come', *IEEE Commun. Mag.*, 1990, **28**, (5), pp. 5–14
2 Nee, R., Prasad, R.: 'OFDM for wireless multimedia communications' (Artech House, 2000)
3 Mallat, S.: 'A wavelet tour of signal processing'' (Academic Press, 1999, 2nd edn.)
4 le Floch, B., Alard, M., Berrou, C.: 'Coded orthogonal frequency division multiplex'. Proc. IEEE, 1995, vol. 83, pp. 982–996
5 Alard, M.: 'Construction of a multicarrier signal'. WO 96/35278, 1996

6 Baas, N.J., Taylor, D.P.: 'Pulse shaping for wireless communication over time- or frequency-selective channels', *IEEE Trans. Commun.*, 2004, **52**, pp. 1477–1479
7 Siohan, P., Roche, C.: 'Cosine-modulated filterbanks based on extended Gaussian function', *IEEE Trans. Signal Process.*, 2000, **48**, (11), pp. 3052–3061
8 Siohan, P., Siclet, C., Lacaille, N.: 'Analysis and design of OFDM/OQAM systems based on filterbank theory', *IEEE Trans. Signal Process.*, 2002, **50**, (5), pp. 1170–1183
9 Vangelista, L., Laurenti, N.: 'Efficient implementation and alternative architecture for OFDM-OQAM systems', *IEEE Trans. Commun.*, 2001, **49**, (4), pp. 664–675
10 Javaudin, J., Bouvet, P.: 'Use of signals in quadrature over OFDM/OQAM'. Proc. IEEE VTC'07, Spring, 2007, pp. 1891–1895
11 Farhang-Boroujeny, B.: 'OFDM vs. filter bank multicarrier', *IEEE Signal Process. Mag.*, 2011, **28**, (3), pp. 92–112
12 Saeedi-Sourck, H., Wu, Y., Bergmans, J., Sadri, S., Farhang-Boroujeny, B.: 'Complexity and performance comparison of filter bank multicarrier and OFDM in uplink of multicarrier multiple access networks', *IEEE Trans. Signal Process.*, 2011, **59**, (4), pp. 1907–1912
13 Lacroix, D., Goudard, N., Alard, M.: 'OFDM with guard interval versus OFDM/offsetQAM for high data rate UMTS downlink transmission'. Proc. VTC'01 Fall, 2001, vol. 4, pp. 2682–2686
14 Du, J., Signell, S.: 'Comparison of CP-OFDM and OFDM/OQAM in doubly dispersive channels'. Proc. FGCN, December 2007
15 Kongara, K., Smith, P., Mann, S.: 'A comparison of CP-OFDM with IOTA-OFDM under typical system imperfections'. Proc. IET WUST, November 2008
16 Lele, C., Javaudin, J.P., Legouable, R., Skrzypczak, A., Siohan, P.: 'Channel estimation methods for preamble-based OFDM/OQAM modulations', *Eur. Trans. Telecommun.*, 2008, pp. 741–750
17 Du, J., Signell, S.: 'Novel preamble-based channel estimation for OFDM/OQAM systems'. Proc. IEEE ICC, June 2009
18 Lin, R., Petropulu, A.: 'Linear precoding assisted blind channel estimation for OFDM systems', *IEEE Trans. Veh. Technol.*, 2005, **54**, (3), pp. 983–995
19 Du, J., Signell, S.: 'Time frequency localization of pulse shaping filters in OFDM/OQAM systems'. Proc. ICICS'07, December 2007
20 Frigo, M., Johnson, S.G.: 'The design and implementation of FFTW3'. Proc. IEEE, February 2005, vol. 93, pp. 216–231
21 O'Hara, B., Petrick, A.: 'IEEE 802.11 handbook: a designer's companion' (IEEE, 2005, 2nd edn.)
22 Liang, Y., Luo, H., Xu, Y., Huang, J.: 'Blind channel estimation based on linear precoding for OFDM systems'. Proc. WICOM., September 2006, pp. 1–4

doi: 10.1049/iet-com.2012.0029